Co-expression network analysis reveals the pivotal role of mitochondrial dysfunction and interferon signature in juvenile dermatomyositis

Danli Zhong [1, 2] , **Chanyuan Wu** [1, 2] , **Jingjing Bai** [1, 2] , **Dong Xu** [1, 2] , **Xiaofeng Zeng** [1, 2] , **Qian Wang** Corresp. [1, 2]

[1] Department of Rheumatology, Peking Union Medical College Hospital, Peking Union Medical College & Chinese Academy of Medical Sciences; National Clinical Research Center for Dermatologic and Immunologic Diseases (NCRC-DID), Beijing, China

[2] Key Laboratory of Rheumatology and Clinical Immunology, Ministry of Education, Beijing, China

Corresponding Author: Qian Wang
Email address: wangqian@pumch.cn

Background: Juvenile dermatomyositis (JDM) is an immune-mediated disease characterized by chronic organ inflammation. The pathogenic mechanisms remain ill-defined; **Methods:** Raw microarray data of JDM were obtained from the gene expression omnibus (GEO) database. Based on GSE3307 dataset with 39 samples, weighted correlation network analysis (WGCNA) was performed to identify key modules associated with pathological state. Functional enrichment analyses were conducted to identify potential mechanisms. Based on the criteria of high connectivity and module membership, candidate hub genes were selected. A protein-protein interaction network was constructed to identify hub genes. Another dataset (GSE11971) was used for the validation of real hub genes. Finally, the real hub genes were used to screen out small-molecule compounds via the Connectivity map database ; **Results:** Three modules were considered as key modules for the pathological state of JDM. Functional enrichment analysis indicated that responses to interferon and metabolism were dysregulated. A total of 45 candidate hub genes were selected according to the pre-established criteria, and 20 genes could differentiate JDM from normal controls by validation of another external dataset (GSE11971). These real hub genes suggested the pivotal role of mitochondrial dysfunction and interferon signature in JDM. Furthermore, drug repositioning highlighted the importance of acacetin, helveticoside, lanatoside C, deferoxamine, LY-294002, tanespimycin and L01AD from downregulated genes with the potential to perturb the development of JDM, while betonicine, felodipine, valproic acid, trichostatin A and sirolimus from upregulated genes provided potentially therapeutic goals for JDM; **Conclusions:** There are 20 real hub genes associated with the pathological state of JDM, suggesting the pivotal role of mitochondrial dysfunction and interferon signature in JDM. This analysis predicted several kinds of small-molecule compounds to treat JDM.

1 # Co-expression network analysis reveals the pivotal role of
2 # mitochondrial dysfunction and interferon signature in
3 # juvenile dermatomyositis

4 Danli Zhong [1], Chanyuan Wu[1], Jingjing Bai[1], Dong Xu[1], Xiaofeng Zeng[1], Qian Wang[1,*]

6 [1] Department of Rheumatology, Peking Union Medical College Hospital, Peking Union Medical
7 College & Chinese Academy of Medical Sciences; National Clinical Research Center for
8 Dermatologic and Immunologic Diseases (NCRC-DID); Key Laboratory of Rheumatology and
9 Clinical Immunology, Ministry of Education, Beijing, China.

11 Corresponding Author:

12 Qian Wang[1,*]

13 Department of Rheumatology, Peking Union Medical College Hospital, Peking Union Medical
14 College & Chinese Academy of Medical Sciences; National Clinical Research Center for
15 Dermatologic and Immunologic Diseases (NCRC-DID); Key Laboratory of Rheumatology and
16 Clinical Immunology, Ministry of Education. No.1 Shuaifuyuan, Beijing 100730, China.

17 Email address: wangqian@pumch.cn

19 ## Abstract

20 **Background:** Juvenile dermatomyositis (JDM) is an immune-mediated disease characterized by
21 chronic organ inflammation. The pathogenic mechanisms remain ill-defined; **Methods:** Raw
22 microarray data of JDM were obtained from the gene expression omnibus (GEO) database. Based
23 on GSE3307 dataset with 39 samples, weighted correlation network analysis (WGCNA) was
24 performed to identify key modules associated with pathological state. Functional enrichment
25 analyses were conducted to identify potential mechanisms. Based on the criteria of high
26 connectivity and module membership, candidate hub genes were selected. A protein-protein
27 interaction network was constructed to identify hub genes. Another dataset (GSE11971) was used
28 for the validation of real hub genes. Finally, the real hub genes were used to screen out small-
29 molecule compounds via the Connectivity map database; **Results:** Three modules were considered
30 as key modules for the pathological state of JDM. Functional enrichment analysis indicated that
31 responses to interferon and metabolism were dysregulated. A total of 45 candidate hub genes were
32 selected according to the pre-established criteria, and 20 genes could differentiate JDM from
33 normal controls by validation of another external dataset (GSE11971). These real hub genes
34 suggested the pivotal role of mitochondrial dysfunction and interferon signature in JDM.
35 Furthermore, drug repositioning highlighted the importance of acacetin, helveticoside, lanatoside
36 C, deferoxamine, LY-294002, tanespimycin and L01AD from downregulated genes with the
37 potential to perturb the development of JDM, while betonicine, felodipine, valproic acid,
38 trichostatin A and sirolimus from upregulated genes provided potentially therapeutic goals for
39 JDM; **Conclusions:** There are 20 real hub genes associated with the pathological state of JDM,

40 suggesting the pivotal role of mitochondrial dysfunction and interferon signature in JDM. This
41 analysis predicted several kinds of small-molecule compounds to treat JDM.

42 **Keywords:** juvenile dermatomyositis; weighted gene co-expression network analysis; hub genes;
43 small-molecule compounds

Introduction

45   Juvenile dermatomyositis (JDM) is a rare chronic childhood-onset autoimmune disease
46 characterized by inflammatory infiltration in small vessels and tissues within skin and muscle. The
47 incidence of JDM is 2-4 per million per year in the United States (Feldman et al. 2008), with
48 female:male ratios ranging from 1.5:1 to 5:1 (Lindsley et al. 1995). The major manifestations of
49 JDM patients consist of symmetrical proximal muscle weakness, skin rashes, and internal organs
50 involvement (Crowe et al. 1982). Up to 30% of JDM may present with calcifications, one of the
51 prognostic factors of long-term disability (Arabshahi et al. 2012; Li & Zhou 2019; Ravelli et al.
52 2010). Adults with JDM in childhood are susceptible to premature cardiovascular damage (Gitiaux
53 et al. 2016).

54   Pathological state and treatment have been reported to affect growth and puberty in the active
55 phase of JDM (Nordal et al. 2019). Ongoing disease activity, irreversible damage, and aggressive
56 immunosuppressive therapy remain major challenges for long-term outcomes and quality of life
57 in JDM patients (Hoeltzel et al. 2014). The etiology of JDM remains ill-defined although genetic
58 and environmental factors are suspected to be involved in its pathogenesis. It has been reported
59 that JDM patients had higher incidence of Epstein-Barr virus infection (Zheng et al. 2019), and
60 the prominent type 1 interferon (IFN) signature was shown to affect the vasculature JDM (De
61 Paepe 2017; Greenberg 2010). Adaptive and innate immune mechanisms involving IFN-
62 associated molecules appear to mediate endothelial tubule-reticular formations and peri-fascicular
63 atrophy.

64   Weighted gene co-expression network analysis (WGCNA) algorithm is a powerful
65 bioinformatic method that mines practical information from gene expression profiles by
66 constructing of gene modules, thereby interpreting the biological significance of a gene
67 (Langfelder & Horvath 2008). WGCNA has been widely used in various diseases (Zhao et al.
68 2010), including malignancies, cardiovascular diseases and autoimmune diseases, where it has
69 provided useful information for understanding pathological process and for discovery of diagnostic
70 and prognostic biomarkers. Nevertheless, WGCNA has never been applied to JDM.

71   Therefore, we used WGCNA for the first time to analyze pathological state and gene
72 expression data in JDM muscular samples to explore and validate hub genes associated with JDM,
73 as well as to predict small-molecule compounds to treat JDM with promising perspectives.

Materials & Methods

75 Data Collection and Differentially Expressed Genes Screening

76   The flowchart of the study is shown in Supplementary Figure 1. Microarray profiles of JDM
77 were retrieved from the Gene Expression Omnibus (GEO, http://www.ncbi.nlm.nih.gov/geo/) of
78 the National Center for Biotechnology Information using the search terms of "juvenile
79 dermatomyositis" restricted in the title. The datasets enrolled in this study must contain musclular
80 specimens with three biological replicates at least. The "affy" package in R environment (version
81 3.6.1) was used to quantile normalize the expression within each dataset (Sasik et al. 2002). The

82 corresponding platforms were applied to annotate each probe according to Entrez ID, and the
83 average expression value was calculated if several probes corresponded to the same Entrez ID.
84 (Supplementary Table 1). The "limma" R package was performed for identifying differentially
85 expressed genes (DEGs) between JDM samples and normal samples under cut-off criteria of false
86 discovery rate (FDR) < 0.05 and |log2fold change| ≥ 1.

87 Co-expression Network Construction

88   The variance of each gene expression value was calculated and the genes with variance ranked
89 in the top 25% were selected for the construction of WGCNA (Langfelder & Horvath 2008). The
90 "WGNCA" package was used to construct the co-expression network. In detail, the function
91 goodSamplesgenes was used to include the qualified genes and samples, followed by choosing an
92 appropriate soft-thresholding power to construct the weighted adjacency matrix by the function
93 pickSoftThreshold. The adjacency matrix was transformed into the topological matrix (TOM), and
94 TOM-based dissimilarity (1-TOM) measure was used to cluster the genes using the flashClust
95 function. Genes in the same module were highly interconnected. Then, phenotype (clinic traits)
96 was imput into the co-expression network, and the following parameters were calculated: module
97 eigengene (ME), gene significance (GS), and module membership (MM). ME represents the
98 significant component in the principal component analysis for each gene module, and MM refers
99 to the connectivity between genes and modules. GS was representative of correlation strength
100 between gene expression and clinical traits, which was calculated by log10 transformation of the
101 P-value (GS = lg P) in the linear regression. Key modules were considered based on the criteria
102 that the correlation coefficient ≥ 0.80 and P-value < 0.05.

103 Functional Enrichment Analysis

104   All genes in key modules were uploaded to the g:Profiler online (Reimand et al. 2007)
105 database to perform Gene Ontology (GO) functional annotation (Ashburner et al. 2000) and the
106 Kyoto encyclopedia of genes and genomes (KEGG) enrichment pathway analysis (Kanehisa &
107 Goto 2000). GO functional analysis consists of biological process (BP), cellular component (CC),
108 and molecular function (MF). Analysis results were extracted under the condition of adjusted P-
109 value < 0.05. The top five terms were visualized if there were more than five terms.

110 Selection and Validation of Hub Genes

111   Genes with high correlation in candidate modules were defined as candidate hub genes. High
112 connectivity was considered when the connectivity ranked in the top 2%. Candidate hub gene met
113 the absolute values of MM > 0.80 and GS > 0.20. After identifying hub genes highly associated
114 with clinical traits, the search tool for the retrieval of interacting genes (STRING) database was
115 used to construct a protein-protein interaction (PPI) network for the candidate hub genes, and
116 molecular complex detection (MCODE, a plugin in Cytoscape) was used to further select the real
117 hub (Shannon et al. 2003; Szklarczyk et al. 2015). Genes with MCODE score ≥ 0 in the PPI
118 network were selected as the final hub genes. A separate dataset GSE11971 was used to validate
119 the differential expression of the final hub genes.

120 Related Small-Molecule Compounds Screening

121   Connectivity map (CMap) database (https://portals.broadinstitute.org/cmap) was used to
122 screen out small molecule compounds based on the real hub genes associated with JDM, because

123 most compounds in this database are the United States Food and Drug Administration-approved
124 drugs, (Lamb et al. 2006). First, real hub genes were divided into upregulated and downregulated
125 groups. Next, these probe sets were used to query the CMap database based on the platform of the
126 Affymetrix Human Genome U133 Plus 2.0 Array
127 (http://www.affymetrix.com/analysis/netaffx/index.affx). Finally, enrichment scores representing
128 similarity were calculated, ranging from −1 to 1. Small molecules generated from up-regulated
129 genes suggested therapeutic goals, while down-regulated genes predicted inhibitors of therapy for
130 the disease. Potential compounds were selected based on connectivity score, *P*-value and
131 correlation.

132 Statistical Analysis

133   Two-tailed Student's t-test was applied to the significance of differences between groups, and
134 P-value less than 0.05 were considered as statistically significant. Statistical analyses were
135 performed using Graphpad Prism 8.0.

136 **Results**

137 Data Collection and Differentially Expressed Genes

138   We employed two datasets on JDM muscular expression profiles. Dataset GSE3307 was used
139 as the training set (Bakay et al. 2006). The original study enrolled 39 muscular biopsy samples,
140 including 21 JDM patients and 18 healthy controls (HC). Dataset GSE11971, including nineteen
141 JDM patients and four normal controls, was used as the validating set (Chen et al. 2008). The gene
142 expression profiles of all tissue samples were analyzed based on the platform of the Affymetrix
143 Human Genome U133 Plus 2.0 Array. A total of 2834 differentially expressed genes between JDM
144 and HC were identified, including 1888 down-regulated genes and 946 up-regulated genes. The
145 DEGs are listed in Supplementary Table 2.

146 Construction of a Weighted Co-expression Network and Identification of Key Modules

147   5103 genes whose variance ranked in the top 25% with 21 JDM samples and 18 control
148 samples in GSE3307 were used for WGCNA construction. The "WGCNA" R package was used
149 for expression matrix of GSE3307, and soft-thresholding power β value equal to 10 was selected
150 to ensure a scale-free network with scale-free R^2 equal to 0.90 (Supplementary Figure 2A-2C)
151 (Langfelder & Horvath 2008). A total of 13 modules were returned by WGCNA analysis (Figure
152 1A-1B).

153   The interaction relationship of 12 modules was analyzed using network heatmap plots (Figure
154 1C). The division of all modules was highly independent from our analysis. The module eigengene
155 dendrogram showed that 12 modules were divided into two clusters, and the adjacency heatmap
156 of eigengene showed a similar result (Figure 2A). Based on the criteria that correlation coefficient
157 ⩾ 0.80, *P* value < 0.05, blue, lightgreen and midnightblue modules were identified as key modules
158 for further analysis (Figure 2B). Therefore, we selected the blue, lightgreen and midnightblue
159 modules for subsequent analysis, to identify the relevance between key modules and the
160 pathological state of JDM with substantial biological significance (Figure 2C-E).

161 Functional and Pathway Enrichment Analysis

162   GO and KEGG pathway enrichment was performed for all genes in the key modules to mine
163 the biological functions associated with JDM. Biological process of GO analysis showed genes in

164 the blue module were associated with generation of SRP-dependent cotranslational protein
165 targeting to membrane, cotranslational protein targeting to membrane, protein targeting to ER,
166 nuclear-transcribed mRNA catabolic process and establishment of protein localization to
167 endoplasmic reticulum; and that in the lightgreen module was relevant to response to type I
168 interferon, type I interferon signaling pathway, cellular response to type I interferon, defense
169 response to virus and response to virus.The top five pathways related to the midnightblue module
170 were cellular response to chemical stimulus, extracellular structure organization, extracellular
171 matrix organization, response to organic substance and cell motility (Figure 3A). Pathway
172 enrichment results of MF and CC in three key modules are presented in Figure 3B-3C. The results
173 of the KEGG pathway enrichment analysis in three modules are shown in Figure 3D.

174 Identification of Hub Genes

175 Based on the criteria that MM > 0.80 and GS > 0.20, a total of 45 DEGs with the high
176 connectivity in key modules were screened as candidate hub genes. Then, a PPI network was
177 constructed for candidate hub genes using Cytoscape, consisting of 42 nodes and 80 edges
178 according to STRING database (Figure 4). We conducted molecular complex detection (MCODE)
179 (a plugin in Cytoscape) analysis for 45 candidate hub genes, and 28 genes (blue = 15, lightgreen
180 = 11, midnightblue = 1) were considered hub genes according to the criteria of MCODE score $\geqslant$
181 0. Table 1 shows 28 hub genes in the three modules.

182 All hub genes were validated using JDM data from another GEO database (GSE11971).
183 Because of the differences in microarray probes used in two data sets, boxplots were used to show
184 the validation results for the final 22 hub genes (Supplementary Figure 3). We found that seven
185 genes, SP110, SAMHD1, IFIT5, PLSCR1, IFI16, MX2 and CLIC1, were significantly upregulated
186 in JDM compared to HC, while thirteen genes, COX5B, COX6A2, COX7C, NDUFA4, NDUFB4,
187 MDH2, ATP5O, ATP5B, RPL21, TPI1, SLC25A3, VDAC1 and EIF4B, were significantly
188 downregulated in JDM in comparison of HC. Figure 5 summarizes the cross-talk pathways
189 involved in the pathogenesis of JDM by hub genes and literature(Miller et al. 2018; Thompson et
190 al. 2017).

191 Related Small-Molecule Compounds Screening

192 The CMap database was used for small molecule drugs screening based on 20 real hub genes
193 associated with JDM . Based on the criterion that the number of instances exceeds five and *P*-
194 value less than 0.05, twelve small-molecule compounds were identified (Table 2). Among these
195 compounds, acacetin, helveticoside, lanatoside C, deferoxamine, famprofazone, tanespimycin and
196 LY-294002 may perturb the development of JDM, while betonicine, felodipine, valproic acid, and
197 sirolimus might provide potentially therapeutic goals for JDM.

Discussion

199

200 In this study, we used WGCNA to construct a co-expression network, detect key gene
201 modules and identify hub genes in JDM for the first time. Our research provides some potential
202 biomarkers or molecular targets for JDM through the Cmap database. We found that three
203 modules highly correlated with JDM. The expression of 28 genes in these three modules showed
204 significant changes in patients with JDM compared to control individuals in the training period,

205   and 20 genes were validated as the real hub genes in the GSE11971 dataset, including the
206   downregulation of NADH dehydrogenase, ATP synthase and cytochrome c oxidase and
207   upregulation of IFN-stimulated genes. However, few of them were identified as biomarkers or
208   crucial genes in JDM yet.

209   Functional enrichment analysis indicated that type I interferon signaling and various virus
210   infection pathways were strengthened in JDM compared to HC, which is consistent with findings
211   of previous studies (Moneta et al. 2019; Piper et al. 2018). IFIT5, IFI16 and MX2, interferon-
212   stimulated genes, both nuclear transcriptional factors, were found to be upregulated in other
213   autoimmune diseases but not in JDM (Wang et al. 2019b; Zhang & Xu 2019). In the present study,
214   we found that interferon-stimulated genes were significantly upregulated in JDM patients, as well
215   as the so-called "interferon signature", demonstrating a possible mechanism that viral mimics or
216   other stimuli may play a crucial role in the pathogenesis of JDM. Viral mimics are thought to
217   participate in the pathogenesis of JDM (Musumeci & Castrogiovanni 2018) and other autoimmune
218   diseases (Christen et al. 2004; Sellami et al. 2019), consistent with the notion that JDM patients
219   have higher rates of viral infections (Tansley et al. 2013; Zheng et al. 2019). This may suggest that
220   the prevention of certain viral infections would decrease the incidence of autoimmunity by
221   inhibiting self-antigenic mimics. NADH dehydrogenase (NDUFA4 and NDUFB4), ATP synthase
222   (ATP5O and ATP5B) and cytochrome c oxidase (COX) family (COX5B, COX6A2 and COX7C)
223   are crucial molecules involved in the oxidative phosphorylation in mitochondrial metabolism, and
224   the decreased levels of these molecules suggested a crucial role of impaired mitochondrial
225   phosphorylation and lower oxidative capacity in the pathogenesis of JDM, accounting for the
226   extremity weakness in JDM patients.

227   Hypoxia caused by suppressed oxidative phosphorylation induces changes in reactive oxygen
228   species (ROS) generation, whereby severe hypoxia in skeletal muscle results in elevated H_2O_2
229   generation. ROS accumulation produced by mitochondrial dysfunctions, in turn, drives type I
230   interferon responses and muscle inflammation, and may thereby self-sustain the disease process
231   (Wang et al. 2019a). Similar to other autoimmune diseases, high-dose glucocorticoids, used alone
232   or in combination with immunosuppressive agents are routine treatment for JDM patients wheras
233   some refractory patients may develop functional limitations. It has been suggested that refractory
234   JDM patients, have lower maximal oxygen uptake(Drinkard et al. 2003; Hicks et al. 2002) than do
235   healthy children and with children with juvenile dermatomyositis in remission(Takken et al. 2008),
236   suggesting that mitochrondrial dysfuction may contribute to the severity of JDM. Current concepts
237   on the therapy of muscle weakness in JDM focus on induction of partial recovery and exposure to
238   serious adverse events (including muscular toxicity). Our data suggest a novel therapeutic
239   perspective for JDM by protecting mitochondria from dysfunction.

240   Bioinformatics combined human and material resources to develop more efficient tools with
241   lower error rates (Irizarry et al. 2003). WGCNA is an efficient approach to construct co-expressed
242   modules and hub genes in several diseases. Previous studies using microarray expression profiles
243   from adult-onset DM patients showed that IFN-stimulated genes were upregulated (i.e. MX2,
244   STAT1 and OAS3), suggesting that the IFN signature overlapped the pathogenesis both in adult
245   and juvenile DM . Nevertheless, mechanisms linked to hypoxia are less prevalent in adult-onset
246   DM, suggesting mitochondrial dysfunctions contribute more to juvenile-onset DM rather than
247   adult-onset DM.

248   We used the CMap database to predict several kinds of small-molecule compounds with
249   promising capacity as therapeutic goals or inhibitors on treatment for JDM. No evidence has

250 demonstrated the direct association between these compounds and JDM, while they hinted indirect
251 link to JDM, according to the literatue. Among these compounds, acacetin, helveticoside,
252 lanatoside C, deferoxamine, famprofazone, tanespimycin and LY-294002 showed negative
253 enrichment scores and thus may have the potential to perturb the development of JDM, while
254 betonicine, felodipine, valproic acid, and sirolimus showed positive enrichment scores and might
255 provide potentially therapeutic goals for JDM. Acacetin, an inhibitor of lipopolysaccharide-
256 induced inflammation, can promote the expansion of Treg cells and supress the differentiation of
257 Th17 cells in a dose-dependent manner in collagen-induced arthritis (Liu et al. 2018).
258 Helveticoside can regulate metabolism and signaling processes as a biologically active component,
259 but little is known in inflammatory reactions (Kim et al. 2015). The iron chelator deferoxamine
260 was shown to reduce mitochondrial oxidative stress in a transient cerebral ischemia model as well
261 as the release of pro-inflammatory molecules including matrix metalloproteinase-9 and hypoxia
262 inducible factor-1 (Im et al. 2012). LY294002, a kind of PI3K inhibitor, has potential against
263 experimental autoimmune myocarditis (Liu et al. 2016). The heat-shock protein 90 inhibitor
264 tanespimycin has been shown to inhibit cutaneous inflammation in experimental epidermolysis
265 bullosa acquisita (Tukaj et al. 2017) and other experimental autoimmune models (Dello Russo et
266 al. 2006). Felodipine, commonly used to treat hypertension and angin, has been evidenced to
267 inhibit oxidative stress and inflammation in endothelial cells, which is consistent with our results
268 (Qi et al. 2017). Valproic acid is a histone deacetylase inhibitor (HDACI), can suppress the
269 inflammatory responses mediated by cytokines, oxidative stress molecules (ROS, NO), activating
270 receptors (NK, Tγδ, and cytotoxic lymphocytes), perforin, granzyme, costimulatory molecules,
271 and autoantibodies(Soria-Castro et al. 2019). Sirolimus can restore immune balance in rheumatoid
272 arthritis patients by expanding the pool of circulating Treg cells(Niu et al. 2019). Our results based
273 on the CMap database might provide hints as to future therapy for JDM; nevertheless, studies in
274 vitro and in vivo are necessary.

275 This study has some limitations. First, this is retrospective, with all data in this study being
276 retrieved from a public database. A multicenter, prospective study is needed to evaluate the
277 significance of these hub genes in terms of long-term outcomes and possible applications of
278 molecular drugs for therapy. Second, experiments in vivo and in vitro are necessary to interpret
279 potential mechanisms of real hub genes and small-molecule compounds for future clinical
280 translation. Third, clinical traits cannot correlate with gene modules when performing WGCNA
281 because of lack of clinical trait data in these GEO datasets.

Conclusions

283   Based on weighted gene co-expression analysis, three key modules and 20 real key genes
284 associated with the pathological state of JDM were identified, suggesting pivotal roles of
285 mitochondrial dysfunction and the interferon signature in JDM. This analysis provides several
286 candidate small-molecule compounds for use as targeted therapy of JDM.

287

Acknowledgements

289 This work was supported by Chinese National Key Technology R&D Program of Ministry of
290 Science and Technology (2017YFC0907604), National Science and Technology Major Project
291 of the Ministry of Science and Technology of China (2019ZX09734001-002-004), Medical
292 and health science and technology innovation project of Chinese Academy of Medical Sciences
293 (2019-I2M-2-008), National Natural Science Foundation of China (81601430, 81471615).

294

295   We would like to acknowledge the GEO, g:Profiler, STRING and CMap databases for free use.

296

Author Contributions

298   Danli Zhong conceived, designed and performed the experiments, analyzed the data, prepared the
299   figures and tables, drafted the work and revised the manuscript.

300   Chanyuan Wu performed the experiments, and revised the manuscript critically for important
301   content.

302   Jingjing Bai used softwares to perform the analysis.

303   Dong Xu and Xiaofeng Zeng analyzed the data, and revised it critically for important content.

304   Qian Wang drafted the work and revised it critically for important content and approved the final
305   draft of the manuscript submitted for review and publication.

306

Data Availability

308   The following information was supplied regarding data availability: Data is available at GEO:
309   GSE3307 and GSE11971.

310

References

312

313   Arabshahi B, Silverman RA, Jones OY, and Rider LG. 2012. Abatacept and sodium thiosulfate
314   for treatment of recalcitrant juvenile dermatomyositis complicated by ulceration and
315   calcinosis. *J Pediatr* 160:520-522. 10.1016/j.jpeds.2011.11.057
316   Ashburner M, Ball CA, Blake JA, Botstein D, Butler H, Cherry JM, Davis AP, Dolinski K, Dwight
317   SS, Eppig JT, Harris MA, Hill DP, Issel-Tarver L, Kasarskis A, Lewis S, Matese JC,
318   Richardson JE, Ringwald M, Rubin GM, and Sherlock G. 2000. Gene ontology: tool for
319   the unification of biology. The Gene Ontology Consortium. *Nat Genet* 25:25-29.
320   10.1038/75556
321   Bakay M, Wang Z, Melcon G, Schiltz L, Xuan J, Zhao P, Sartorelli V, Seo J, Pegoraro E,
322   Angelini C, Shneiderman B, Escolar D, Chen YW, Winokur ST, Pachman LM, Fan C,
323   Mandler R, Nevo Y, Gordon E, Zhu Y, Dong Y, Wang Y, and Hoffman EP. 2006. Nuclear
324   envelope dystrophies show a transcriptional fingerprint suggesting disruption of Rb-
325   MyoD pathways in muscle regeneration. *Brain* 129:996-1013. 10.1093/brain/awl023
326   Chen YW, Shi R, Geraci N, Shrestha S, Gordish-Dressman H, and Pachman LM. 2008.
327   Duration of chronic inflammation alters gene expression in muscle from untreated girls
328   with juvenile dermatomyositis. *BMC Immunol* 9:43. 10.1186/1471-2172-9-43
329   Christen U, Edelmann KH, McGavern DB, Wolfe T, Coon B, Teague MK, Miller SD, Oldstone
330   MB, and von Herrath MG. 2004. A viral epitope that mimics a self antigen can accelerate
331   but not initiate autoimmune diabetes. *J Clin Invest* 114:1290-1298. 10.1172/jci22557
332   Crowe WE, Bove KE, Levinson JE, and Hilton PK. 1982. Clinical and pathogenetic implications
333   of histopathology in childhood polydermatomyositis. *Arthritis Rheum* 25:126-139.
334   10.1002/art.1780250203

335   De Paepe B. 2017. Vascular changes and perifascicular muscle fiber damage in
336   dermatomyositis: another question of the chicken or the egg that is on our mind. *Ann*
337   *Transl Med* 5:22. 10.21037/atm.2016.12.68
338   Dello Russo C, Polak PE, Mercado PR, Spagnolo A, Sharp A, Murphy P, Kamal A, Burrows FJ,
339   Fritz LC, and Feinstein DL. 2006. The heat-shock protein 90 inhibitor 17-allylamino-17-
340   demethoxygeldanamycin suppresses glial inflammatory responses and ameliorates
341   experimental autoimmune encephalomyelitis. *J Neurochem* 99:1351-1362.
342   10.1111/j.1471-4159.2006.04221.x
343   Drinkard BE, Hicks J, Danoff J, and Rider LG. 2003. Fitness as a determinant of the oxygen
344   uptake/work rate slope in healthy children and children with inflammatory myopathy. *Can*
345   *J Appl Physiol* 28:888-897. 10.1139/h03-063
346   Feldman BM, Rider LG, Reed AM, and Pachman LM. 2008. Juvenile dermatomyositis and other
347   idiopathic inflammatory myopathies of childhood. *Lancet* 371:2201-2212.
348   10.1016/s0140-6736(08)60955-1
349   Gitiaux C, De Antonio M, Aouizerate J, Gherardi RK, Guilbert T, Barnerias C, Bodemer C,
350   Brochard-Payet K, Quartier P, Musset L, Chazaud B, Desguerre I, and Bader-Meunier B.
351   2016. Vasculopathy-related clinical and pathological features are associated with severe
352   juvenile dermatomyositis. *Rheumatology (Oxford)* 55:470-479.
353   10.1093/rheumatology/kev359
354   Greenberg SA. 2010. Dermatomyositis and type 1 interferons. *Curr Rheumatol Rep* 12:198-203.
355   10.1007/s11926-010-0101-6
356   Hicks JE, Drinkard B, Summers RM, and Rider LG. 2002. Decreased aerobic capacity in
357   children with juvenile dermatomyositis. *Arthritis Rheum* 47:118-123. 10.1002/art.10237
358   Hoeltzel MF, Oberle EJ, Robinson AB, Agarwal A, and Rider LG. 2014. The presentation,
359   assessment, pathogenesis, and treatment of calcinosis in juvenile dermatomyositis. *Curr*
360   *Rheumatol Rep* 16:467. 10.1007/s11926-014-0467-y
361   Im DS, Jeon JW, Lee JS, Won SJ, Cho SI, Lee YB, and Gwag BJ. 2012. Role of the NMDA
362   receptor and iron on free radical production and brain damage following transient middle
363   cerebral artery occlusion. *Brain Res* 1455:114-123. 10.1016/j.brainres.2012.03.025
364   Irizarry RA, Hobbs B, Collin F, Beazer-Barclay YD, Antonellis KJ, Scherf U, and Speed TP.
365   2003. Exploration, normalization, and summaries of high density oligonucleotide array
366   probe level data. *Biostatistics* 4:249-264. 10.1093/biostatistics/4.2.249
367   Kanehisa M, and Goto S. 2000. KEGG: kyoto encyclopedia of genes and genomes. *Nucleic*
368   *Acids Res* 28:27-30. 10.1093/nar/28.1.27
369   Kim BY, Lee J, and Kim NS. 2015. Helveticoside is a biologically active component of the seed
370   extract of Descurainia sophia and induces reciprocal gene regulation in A549 human
371   lung cancer cells. *BMC Genomics* 16:713. 10.1186/s12864-015-1918-1
372   Lamb J, Crawford ED, Peck D, Modell JW, Blat IC, Wrobel MJ, Lerner J, Brunet JP,
373   Subramanian A, Ross KN, Reich M, Hieronymus H, Wei G, Armstrong SA, Haggarty SJ,
374   Clemons PA, Wei R, Carr SA, Lander ES, and Golub TR. 2006. The Connectivity Map:
375   using gene-expression signatures to connect small molecules, genes, and disease.
376   *Science* 313:1929-1935. 10.1126/science.1132939
377   Langfelder P, and Horvath S. 2008. WGCNA: an R package for weighted correlation network
378   analysis. *BMC Bioinformatics* 9:559. 10.1186/1471-2105-9-559
379   Li J, and Zhou Z. 2019. Calcinosis in Juvenile Dermatomyositis. *N Engl J Med* 381:e31.
380   10.1056/NEJMicm1809669
381   Lindsley C, Laxer RM, Cassidy JT, and Petty R. 1995. Textbook of Pediatric Rheumatology [M].
382   *Philadelphia: Elsevier Saunders*:539-546. 10.1016/C2009-0-42830-7
383   Liu HS, Zhang J, Guo JL, Lin CY, and Wang ZW. 2016. Phosphoinositide 3-kinase inhibitor
384   LY294002 ameliorates the severity of myosin-induced myocarditis in mice. *Curr Res*
385   *Transl Med* 64:21-27. 10.1016/j.retram.2016.01.012

386 Liu L, Yang J, Zu B, Wang J, Sheng K, Zhao L, and Xu W. 2018. Acacetin regulated the
387   reciprocal differentiation of Th17 cells and Treg cells and mitigated the symptoms of
388   collagen-induced arthritis in mice. *Scand J Immunol* 88:e12712. 10.1111/sji.12712
389 Miller FW, Lamb JA, Schmidt J, and Nagaraju K. 2018. Risk factors and disease mechanisms in
390   myositis. *Nat Rev Rheumatol* 14:255-268. 10.1038/nrrheum.2018.48
391 Moneta GM, Pires Marafon D, and Marasco E. 2019. Muscle Expression of Type I and Type II
392   Interferons Is Increased in Juvenile Dermatomyositis and Related to Clinical and
393   Histologic Features. 71:1011-1021. 10.1002/art.40800
394 Musumeci G, and Castrogiovanni P. 2018. Expression of the OAS Gene Family Is Highly
395   Modulated in Subjects Affected by Juvenile Dermatomyositis, Resembling an Immune
396   Response to a dsRNA Virus Infection. 19. 10.3390/ijms19092786
397 Niu HQ, Li ZH, Zhao WP, Zhao XC, Zhang C, Luo J, Lu XC, Gao C, Wang CH, and Li XF. 2019.
398   Sirolimus selectively increases circulating Treg cell numbers and restores the Th17/Treg
399   balance in rheumatoid arthritis patients with low disease activity or in DAS28 remission
400   who previously received conventional disease-modifying anti-rheumatic drugs. *Clin Exp*
401   *Rheumatol*.
402 Nordal E, Pistorio A, Rygg M, Giancane G, Maghnie M, Di Iorgi N, Flemming K, Hofer M, Melo-
403   Gomes JA, Bica B, Brunner J, Dannecker G, Gerloni V, Harjacek M, Huppertz HI,
404   Pratsidou-Gertsi P, Nielsen S, Stanevicha V, Ten Cate R, Vougiouka O, Pastore S,
405   Simonini G, Ravelli A, Martini A, and Ruperto N. 2019. Growth and puberty in juvenile
406   dermatomyositis: a longitudinal cohort study. *Arthritis Care Res (Hoboken)*.
407   10.1002/acr.24065
408 Piper CJM, Wilkinson MGL, Deakin CT, Otto GW, Dowle S, Duurland CL, Adams S, Marasco E,
409   Rosser EC, Radziszewska A, Carsetti R, Ioannou Y, Beales PL, Kelberman D, Isenberg
410   DA, Mauri C, Nistala K, and Wedderburn LR. 2018. CD19(+)CD24(hi)CD38(hi) B Cells
411   Are Expanded in Juvenile Dermatomyositis and Exhibit a Pro-Inflammatory Phenotype
412   After Activation Through Toll-Like Receptor 7 and Interferon-alpha. *Front Immunol*
413   9:1372. 10.3389/fimmu.2018.01372
414 Qi J, Zheng JB, Ai WT, Yao XW, Liang L, Cheng G, Shou XL, and Sun CF. 2017. Felodipine
415   inhibits ox-LDL-induced reactive oxygen species production and inflammation in human
416   umbilical vein endothelial cells. *Mol Med Rep* 16:4871-4878. 10.3892/mmr.2017.7181
417 Ravelli A, Trail L, Ferrari C, Ruperto N, Pistorio A, Pilkington C, Maillard S, Oliveira SK,
418   Sztajnbok F, Cuttica R, Beltramelli M, Corona F, Katsicas MM, Russo R, Ferriani V,
419   Burgos-Vargas R, Magni-Manzoni S, Solis-Valleoj E, Bandeira M, Zulian F, Baca V,
420   Cortis E, Falcini F, Alessio M, Alpigiani MG, Gerloni V, Saad-Magalhaes C, Podda R,
421   Silva CA, Lepore L, Felici E, Rossi F, Sala E, and Martini A. 2010. Long-term outcome
422   and prognostic factors of juvenile dermatomyositis: a multinational, multicenter study of
423   490 patients. *Arthritis Care Res (Hoboken)* 62:63-72. 10.1002/acr.20015
424 Reimand J, Kull M, Peterson H, Hansen J, and Vilo J. 2007. g:Profiler--a web-based toolset for
425   functional profiling of gene lists from large-scale experiments. *Nucleic Acids Res*
426   35:W193-200. 10.1093/nar/gkm226
427 Sasik R, Calvo E, and Corbeil J. 2002. Statistical analysis of high-density oligonucleotide arrays:
428   a multiplicative noise model. *Bioinformatics* 18:1633-1640.
429   10.1093/bioinformatics/18.12.1633
430 Sellami M, Saidane O, Mahmoud I, Tekaya AB, Tekaya R, and Abdelmoula L. 2019. Etiological
431   features of liver involvement in rheumatoid arthritis. *Curr Rheumatol Rev*.
432   10.2174/1573397115666191007121605
433 Shannon P, Markiel A, Ozier O, Baliga NS, Wang JT, Ramage D, Amin N, Schwikowski B, and
434   Ideker T. 2003. Cytoscape: a software environment for integrated models of
435   biomolecular interaction networks. *Genome Res* 13:2498-2504. 10.1101/gr.1239303

436 Soria-Castro R, Schcolnik-Cabrera A, Rodriguez-Lopez G, Campillo-Navarro M, Puebla-Osorio
437   N, Estrada-Parra S, Estrada-Garcia I, Chacon-Salinas R, and Chavez-Blanco AD. 2019.
438   Exploring the Drug Repurposing Versatility of Valproic Acid as a Multifunctional
439   Regulator of Innate and Adaptive Immune Cells. *J Immunol Res* 2019:9678098.
440   10.1155/2019/9678098
441 Szklarczyk D, Franceschini A, Wyder S, Forslund K, Heller D, Huerta-Cepas J, Simonovic M,
442   Roth A, Santos A, Tsafou KP, Kuhn M, Bork P, Jensen LJ, and von Mering C. 2015.
443   STRING v10: protein-protein interaction networks, integrated over the tree of life. *Nucleic*
444   *Acids Res* 43:D447-452. 10.1093/nar/gku1003
445 Takken T, van der Net J, Engelbert RH, Pater S, and Helders PJ. 2008. Responsiveness of
446   exercise parameters in children with inflammatory myositis. *Arthritis Rheum* 59:59-64.
447   10.1002/art.23250
448 Tansley SL, McHugh NJ, and Wedderburn LR. 2013. Adult and juvenile dermatomyositis: are
449   the distinct clinical features explained by our current understanding of serological
450   subgroups and pathogenic mechanisms? *Arthritis Res Ther* 15:211. 10.1186/ar4198
451 Thompson C, Piguet V, and Choy E. 2017. The pathogenesis of dermatomyositis. *Br J*
452   *Dermatol*. 10.1111/bjd.15607
453 Tukaj S, Bieber K, Kleszczynski K, Witte M, Cames R, Kalies K, Zillikens D, Ludwig RJ, Fischer
454   TW, and Kasperkiewicz M. 2017. Topically Applied Hsp90 Blocker 17AAG Inhibits
455   Autoantibody-Mediated Blister-Inducing Cutaneous Inflammation. *J Invest Dermatol*
456   137:341-349. 10.1016/j.jid.2016.08.032
457 Wang HW, Zhang Y, Tan PP, Jia LS, Chen Y, and Zhou BH. 2019a. Mitochondrial respiratory
458   chain dysfunction mediated by ROS is a primary point of fluoride-induced damage in
459   Hepa1-6 cells. *Environ Pollut* 255:113359. 10.1016/j.envpol.2019.113359
460 Wang X, Zhang Z, Zhao W, Li Z, Yang G, Liu P, Jia J, Shi H, Liu M, Liu T, Gu J, Wan L, Teng J,
461   Liu H, Cheng X, Ye J, Su Y, Sun Y, Gong W, Yang C, and Hu Q. 2019b.
462   Cytomegalovirus Infection May Trigger Adult-Onset Still's Disease Onset or Relapses. *J*
463   *Cell Biochem* 10:898. 10.1002/jcb.29001
464 10.3389/fimmu.2019.00898
465 Zhang L, and Xu P. 2019. Identification of differentially expressed genes in primary Sjogren's
466   syndrome. 120:17368-17377. 10.1002/hep.30897
467 10.1002/jcb.29001
468 Zhao W, Langfelder P, Fuller T, Dong J, Li A, and Hovarth S. 2010. Weighted gene
469   coexpression network analysis: state of the art. *J Biopharm Stat* 20:281-300.
470   10.1080/10543400903572753
471 Zheng Q, Zhu K, Gao CN, Xu YP, and Lu MP. 2019. Prevalence of Epstein-Barr virus infection
472   and characteristics of lymphocyte subsets in newly onset juvenile dermatomyositis.
473   10.1007/s12519-019-00314-7

474

475

476 Figure legends

477   **Figure 1.** Construction of WGCNA modules. (**A**) Dendrogram of module eigengenes
478   based on dissimilarity measure (1-TOM); (**B**) Cluster dendrogram of the genes with
479   variance ranked in the top 25% in GSE3307 dataset. Each color represents one module.
480   The blue module contained the most genes (n = 1549), followed by lightgreen (n = 941),
481   black (n = 428), darkgrey (n = 367), midnightblue (n = 280), darkred (n = 251), magenta
482   (n = 211), purple (n = 196), salmon (n = 172), lightcyan (n = 169), darkgreen (n = 100),
483   and darkturquoise (n = 96) modules. The 343 genes that could not be incorporated into

484   any modules belonged to the grey module, and were removed in the subsequent analysis;
485   (**C**) Network heatmap plots of genes selected for WGCNA construction. The depth of
486   yellow in the middle of the figure indicated the degree of correlation between pair-wise
487   genes.

488   **Figure 2.** Relationship between modules and clinical traits. (**A**) Module eigengene
489   dendrogram and Adjacency heatmap. (**B**) Heatmap of the module-trait relationships. (**C-**
490   **E**) Scatter plots of module eigengenes in blue(**C**), lightgreen (**D**) and midnightblue (**E**)
491   modules.

492   **Figure 3.** Top 5 terms of GO and KEGG pathway enrichment analysis in blue, lightgreen
493   and midnightblue modules. The horizontal axis represents the gene ratio, and the vertical
494   axis indicates the term of GO/KEGG signaling pathway, and the change of color from
495   blue to red indicates the change of significance from low to high. (**A**) Biological function;
496   (**B**) cellular component; (**C**) molecular function; (**D**) KEGG enrichment pathway.

497   **Figure 4.** Protein-protein interaction network of 45 hub genes. Different shapes represent
498   various clusters constructed by molecular complex detection (MCODE). i.e. ellipses
499   represent cluster 1 and triangles represent cluster 2. The color changes from dark brown
500   to light brown indicate the MCODE score changes from high to low.

501   **Figure 5.** Cross-talk pathways involved in JDM interfered by hub genes and reference.
502   Enviromental factors (such as the invasion of virus) stimulate receptors to pathogen-
503   associated molecular patterns (PAMPs) or cytokines on skeletal muscle cells and vascular
504   endothelial cells, followed by the activation of DNA-cGAS-STING axis or RNA-
505   MDA5/RIG-I-MAVS axis, thereby inducing the transcription of interferon-stimulated
506   genes and other genes by phosphorylating IRF3/7, ultimately leading to inflammatory
507   infiltration in blood vessels as well as skeletal muscle weakness. The dysfunction of
508   metabolic signallings through cytokine receptors (for example, the type I interferon
509   receptor (IFNAR) and/or IL-1 receptor (IL-1R)) activated oxidative phosphorylation in
510   mitochondria, leading to the accumulation of reactive oxygen species (ROS), potentially
511   resulting in energy-generating deficits in skeletal muscles. The hub genes involved in the
512   pathogenesis of JDM are as follows: IFN-stimulated genes: IFIT5, IFI16 and MX2;
513   Cytochrome c oxidase: COX5B, COX6A2 and COX7C; NADH dehydrogenase:
514   NDUFA4 and NDUFB4; ATP synthase: ATP5B and ATP5O.

515   **Supplementary Figure 1.** The flowchart of this study.

516   **Supplementary Figure 2.** Clustering dendrogram of all samples and determination of
517   soft-thresholding power. (**A**) Sample clustering was conducted to detect outliers. All
518   samples are located in the clusters and pass the cutoff thresholds. (**B**) Analysis of the
519   scale-free fit index for various soft-thresholding powers (β). (**C**) Analysis of the mean
520   connectivity for various soft-thresholding powers.

521   **Supplementary Figure 3.** Boxplots of 22 hub genes. (**A**) ATP5O, ATP5B, NDUFV2,
522   COX7C, COX5B, NDUFB4 and COX6A2; (**B**) NDUFA4, VDAC1, SLC25A3, MDH2,

523   TPI1, RPL21, MRPS7 and MX2; (**C**) SAMHD1, EIF4B, IFIT5, SP110, IFI16, PLSCR1,
524   and CLIC1.

Figure 1

Figure 1

Construction of WGCNA modules. (**A**) Dendrogram of module eigengenes based on dissimilarity measure (1-TOM); (**B**) Cluster dendrogram of the genes with variance ranked in the top 25% in GSE3307 dataset. Each color represents one module; (**C**) Network heatmap plots of genes selected for WGCNA construction. The depth of yellow in the middle of the figure indicated the degree of correlation between pair-wise genes.

Figure 2

Figure 2

Relationship between modules and clinical traits. (**A**) Module eigengene dendrogram and Adjacency heatmap. (**B**) Heatmap of the module-trait relationships. (**C-E**) Scatter plots of module eigengenes in blue(**C**), lightgreen (**D**) and midnightblue (**E**) modules.
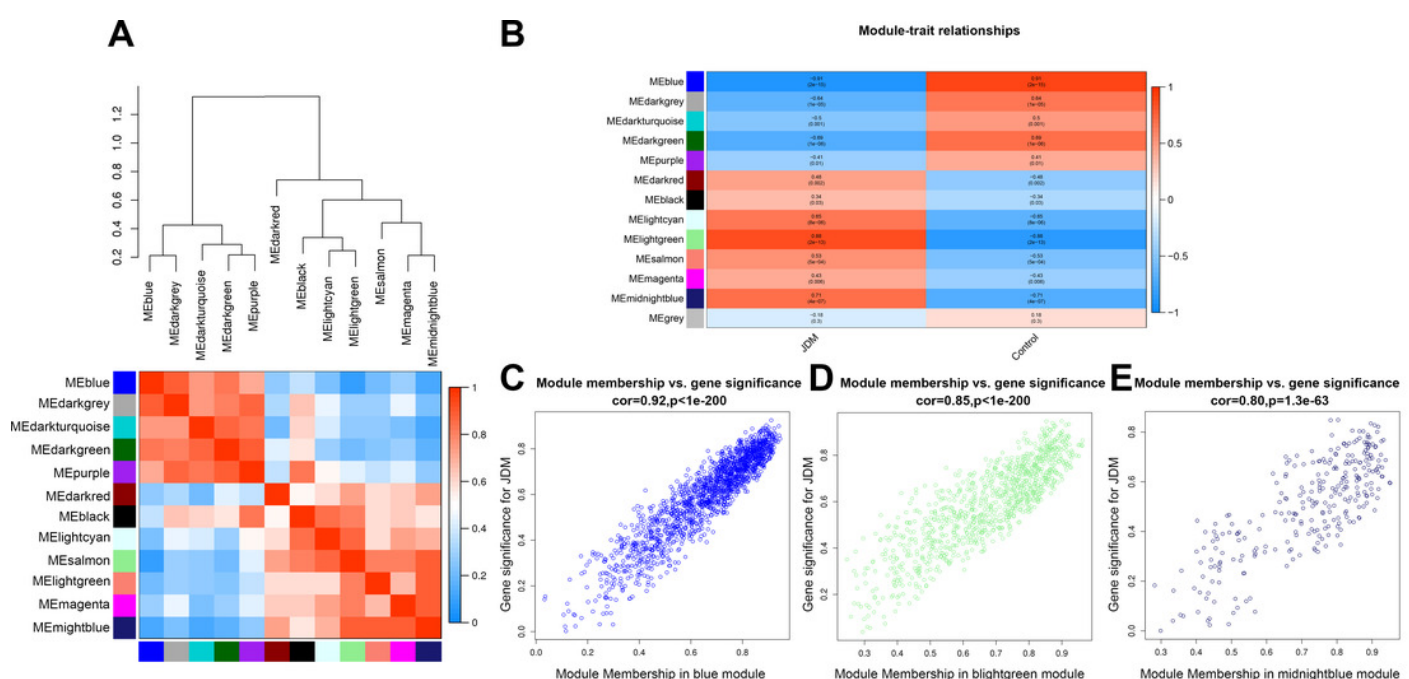
Figure 3

Figure 3

Top 5 terms of GO and KEGG pathway enrichment analysis in blue, lightgreen and midnightblue modules. The horizontal axis represents the gene ratio, and the vertical axis indicates the term of GO/KEGG signaling pathway, and the change of color from blue to red indicates the change of significance from low to high. (**A**) Biological function; (**B**) cellular component; (**C**) molecular function; (**D**) KEGG enrichment pathway.

Figure 4

Figure 4

Protein-protein interaction network of 45 hub genes. Different shapes represent various clusters constructed by molecular complex detection (MCODE). i.e. ellipses represent cluster 1 and triangles represent cluster 2. The color changes from dark brown to light brown indicate the MCODE score changes from high to low.
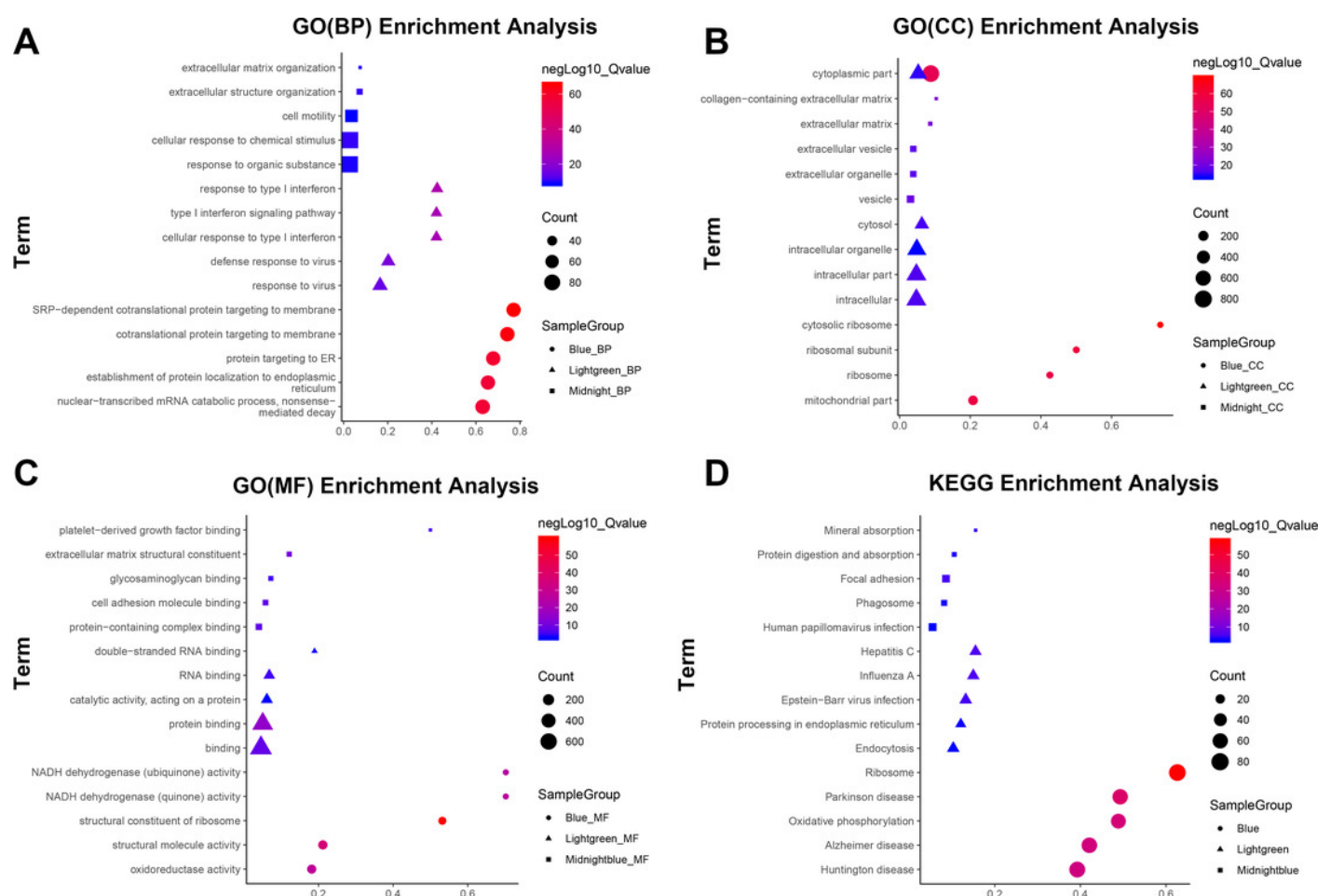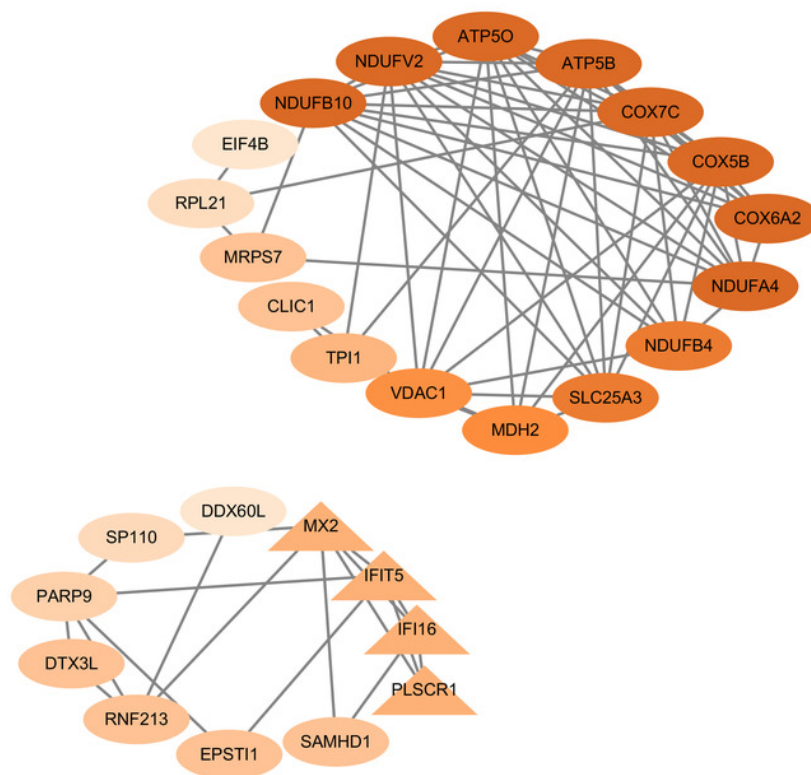
Figure 5

Figure 5

Cross-talk pathways involved in JDM interfered by hub genes and reference. Enviromental factors (such as the invasion of virus) stimulate receptors to pathogen-associated molecular patterns (PAMPs) or cytokines on skeletal muscle cells and vascular endothelial cells, followed by the activation of DNA-cGAS-STING axis or RNA-MDA5/RIG-I-MAVS axis, thereby inducing the transcription of interferon-stimulated genes and other genes by phosphorylating IRF3/7, ultimately leading to inflammatory infiltration in blood vessels as well as skeletal muscle weakness. The dysfunction of metabolic signallings through cytokine receptors (for example, the type I interferon receptor (IFNAR) and/or IL-1 receptor (IL-1R)) activated oxidative phosphorylation in mitochondria, leading to the accumulation of reactive oxygen species (ROS), potentially resulting in energy-generating deficits in skeletal muscles. The hub genes involved in the pathogenesis of JDM are as follows: IFN-stimulated genes: IFIT5, IFI16 and MX2; Cytochrome c oxidase: COX5B, COX6A2 and COX7C; NADH dehydrogenase: NDUFA4 and NDUFB4 ; ATP synthase: ATP5B and ATP5O.
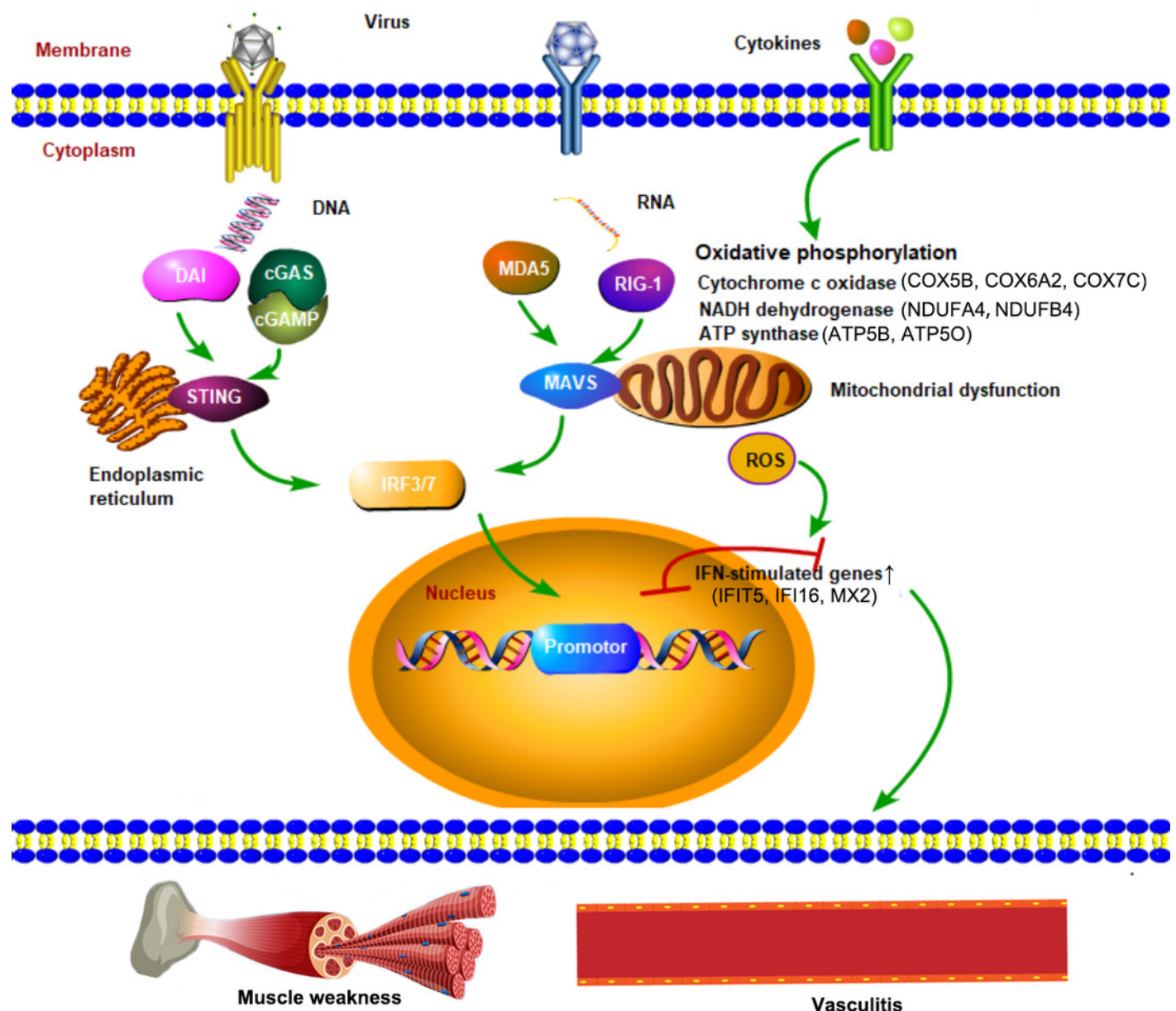
Table 1

1 **Table 1.** Hub genes identified by co-expression and MCODE methods

Gene	GS.JDM	MM	MCODE_Score	regulation	module
ATP5O	-0.860	0.905	7.0	down	blue
ATP5B	-0.903	0.892	7.0	down	blue
NDUFV2	-0.792	0.912	7.0	no sig	blue
NDUFB10	-0.844	0.946	7.0	NA	blue
COX7C	-0.784	0.919	7.0	down	blue
COX5B	-0.830	0.937	7.0	down	blue
NDUFB4	-0.805	0.922	6.0	down	blue
COX6A2	-0.841	0.922	7.0	down	blue
NDUFA4	-0.833	0.833	7.0	down	blue
VDAC1	-0.880	0.896	4.8	down	blue
SLC25A3	-0.859	0.903	6.0	down	blue
MDH2	-0.851	0.921	5.0	down	blue
TPI1	-0.899	-0.899	2.7	down	blue
RPL21	-0.827	0.915	0.5	down	blue
MRPS7	-0.842	0.916	2.0	no sig	blue
PARP9	0.844	0.950	1.2	NA	lightgreen
DTX3L	0.844	0.961	2.0	NA	lightgreen
MX2	0.930	0.913	3.0	up	lightgreen
SAMHD1	0.846	0.954	2.0	up	lightgreen
RNF213	0.841	0.961	2.0	NA	lightgreen
EIF4B	-0.885	-0.919	0.0	down	lightgreen
IFIT5	0.934	0.921	3.0	up	lightgreen
SP110	0.864	0.963	0.7	up	lightgreen
IFI16	0.881	0.913	3.0	up	lightgreen
PLSCR1	0.879	0.922	3.0	up	lightgreen
EPSTI1	0.797	0.925	2.0	NA	lightgreen
DDX60L	0.846592	0.923402	0.0	NA	lightgreen
CLIC1	0.768	0.933	2.0	up	midnightgreen

Table 2

1   **Table 2.** Small molecule drugs screening based on CMap database

Cmap name and cell line	Mean score	Number	Enrichment	*P*-value	Specificity	Percent non-null
0175029-0000	-0.696	6	-0.982	0	0	100
acacetin	-0.465	6	-0.785	0.00018	0	100
helveticoside	-0.494	6	-0.754	0.00044	0.013	83
lanatoside C	-0.424	6	-0.7	0.00167	0.0638	66
betonicine	0.239	6	0.676	0.00312	0.0065	66
deferoxamine	-0.345	8	-0.556	0.00726	0.0184	62
famprofazone	-0.203	6	-0.557	0.02862	0.1035	50
felodipine	0.213	7	0.511	0.03088	0.1089	71
trichostatin A - HL60	0.283	34	0.623	0	0.0798	52
trichostatin A - MCF7	0.172	92	0.399	0	0.673	56
LY-294002 - PC3	-0.243	12	-0.494	0.00325	0.2249	58
valproic acid - HL60	0.254	14	0.417	0.01034	0.1812	50
sirolimus - HL60	0.305	10	0.534	0.00359	0.0347	70
vorinostat - MCF7	0.22	7	0.5	0.0378	0.7655	71